Analytical and Numerical Evaluation of Wall Thermal Boundary Conditions in Free Convective Thin Plates with Internal Heat Generation

Moon Won Song[a,b*]
[a]*High-enthlapy Plasma Research Center, Jeonbuk National University*
[b]*School of Convergence Defense Industry, Jeonbuk National University*
[*]*Corresponding author: moon1song@jbnu.ac.kr*

***Keywords :** free convection, volumetric heat generation, thermal boundary condition, perturbation method

1. Introduction

Free convection in vertical flat plates is crucial in various engineering applications, including the thermal design of research reactor fuel plates. Unlike traditional boundary conditions of uniform wall temperature (UWT) or uniform heat flux (UHF), nuclear fuels generally involve volumetric heat generation rather than being limited to UWT or UHF conditions. This requires a systematic approach to assess whether the heating plate's thermal boundary condition aligns more closely with UWT or UHF conditions.

In previous studies, peak temperature correlations were mainly developed under either UWT or UHF conditions[1]. However, for plates with identical volumetric heat generation, the peak temperature varies significantly depending on whether UWT or UHF assumptions are used [2].

This study proposes a quantitative scaling criterion to determine which boundary condition more accurately describes a given thermal system. The approach is based on analytical derivation using perturbation analysis, numerical solutions via the Runge-Kutta method

2. Analytical Derivation

To assess the wall thermal boundary conditions of free-convective plates with volumetric heat generation, the governing equations of conjugate heat transfer were examined using perturbation methods.

The thermal boundary layer thickness (δ_T) in free convection is typically proportional to the -1/4th power of the Rayleigh number for UWT and the -1/5th power of the q"-based Rayleigh number for UHF conditions. These relationships determine how heat flux and temperature vary along the plate.

To define the Rayleigh number converted from volumetric heat generation (q''') to the UHF condition, the temperature difference in Eq. (1) is changed to $(q'''d\delta_T)/k$ as follows;

$$\delta_{T,UHF,q'''} \sim LRa_{UHF,q'''}^{-1/5}$$
$$\text{where } Ra_{UHF,q'''} = \frac{g\beta q''' dL^4}{\alpha\nu k},\ \Delta T_{UHF,q'''} = \frac{q''' dL}{k}, d = \frac{t}{2} \tag{1}$$

From now on, the longitudinal length of a plate (x) was replaced by L. For a simple non-dimensionalization of the governing equations, the Rayleigh number ($Ra_{UWT,q'''}$), converted from volumetric heat generation to the UWT condition, is introduced with a power of -1/4th to δ_T, as shown in Eq. (2).

$$\delta_{T,UWT,q'''} \sim LRa_{UWT,q'''}^{-1/4}$$
$$\text{where } Ra_{UWT,q'''} = Ra_{UHF,q'''}^{0.8} = \frac{g\beta\Delta T_{UWT,q'''}L^3}{\alpha\nu} \tag{2}$$
$$\text{and } \Delta T_{UWT,q'''} = \Delta T_{UHF,q'''} / Ra_{UHF,q'''}^{0.2}$$

Based on the Rayleigh number converted from the volumetric heat generation to the UWT condition, the ratio of free convection to longitudinal conduction in a solid ($s_{conj,mo}$) can be defined using Eq. (3)

$$\sigma_{conj,\text{mo}} \sim \frac{\text{free convection}}{\text{longitudinal conduction}}$$
$$\sigma_{conj,\text{mo}} = \frac{k}{\delta_T}\frac{L}{k_{solid}} = \frac{kRa_{UWT,q'''}^{1/4}}{k_{solid}} = \frac{k}{k_{solid}}\left(\frac{g\beta q''' dL^4}{\alpha\nu k}\right)^{0.2} \tag{3}$$

Using parameters in Eq. (3) and the similarity variables in Eq. (4), the governing equations were transformed into non-dimensional equations (Eqs. (5)–(12)) [3]. The geometrical interpretation are shown in Fig. 1.

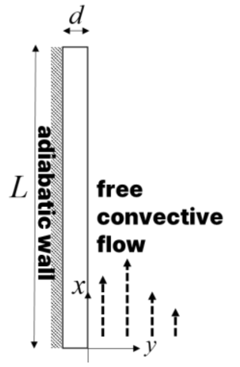

Fig. 1. Geometrical interpretation for free convective/conductive conjugate heat transfer

$$\chi = \frac{x}{L},\ \eta = Ra_{UWT,q'''}^{1/4}\frac{y}{L\chi^{1/4}},\ z = \frac{y}{d},\ f = \frac{\Pr\psi}{\nu Ra_{UWT,q'''}^{1/4}\chi^{3/4}}, \tag{4}$$
$$\theta = \frac{T - T_\infty}{\Delta T_{UWT,q'''}},\ \theta_{solid} = \frac{T_{solid} - T_\infty}{\Delta T_{UWT,q'''}}$$

Non-dimensional governing equations

$$\frac{\partial^3 f}{\partial\eta^3}+\theta=\frac{1}{\Pr}\left[\frac{1}{2}\left(\frac{\partial f}{\partial\eta}\right)^2-\frac{3}{4}f\frac{\partial^2 f}{\partial\eta^2}+\chi\left(\frac{\partial f}{\partial\eta}\frac{\partial^2 f}{\partial\chi\partial\eta}-\frac{\partial f}{\partial\chi}\frac{\partial^2 f}{\partial\eta^2}\right)\right] \quad (5)$$

$$\frac{\partial^2\theta}{\partial\eta^2}+\frac{3}{4}f\frac{\partial\theta}{\partial\eta}=\chi\left(\frac{\partial f}{\partial\eta}\frac{\partial\theta}{\partial\chi}-\frac{\partial f}{\partial\chi}\frac{\partial\theta}{\partial\eta}\right) \quad (6)$$

$$\frac{k_{solid}d}{kRa_{UWT,q'''}{}^{1/4}L}\left(\frac{\partial^2\theta_{solid}}{\partial\chi^2}+\frac{L^2}{h^2}\frac{\partial^2\theta_{solid}}{\partial z^2}\right)+1=0 \quad (7)$$

Boundary conditions

$$\frac{\partial\theta_{solid}}{\partial z}=0 \text{ at } z=-1 \quad (8)$$

$$\frac{\partial\theta_{solid}}{\partial z}-\frac{k_{solid}d}{kRa_{UWT,q'''}^{1/4}L\chi^{1/4}}\frac{\partial\theta}{\partial\eta}=0 \text{ at } z=0 \quad (9)$$

$$\frac{\partial\theta_{solid}}{\partial\chi}=0 \text{ for } \chi=0 \text{ and } \chi=1 \quad (10)$$

$$\frac{\partial f}{\partial\eta}=\theta=0 \text{ for } \eta\to\infty \quad (11)$$

$$f=\frac{\partial f}{\partial\eta}=\theta-\theta_{solid} \text{ at } \eta=z=0 \quad (12)$$

Eq. (7) was integrated along the z-direction to determine the surface heat flux at the interface between the solid and fluid. Assuming that the plate was sufficiently thin, the average temperature in the z-direction was equal to the wall temperature.

$$\frac{d}{\sigma_{conj,mo}L}\frac{\partial^2\theta_{solid}}{\partial\chi^2}+1=-\frac{1}{\chi^{1/4}}\left.\frac{\partial\theta}{\partial\eta}\right|_{\eta=0} \quad (13)$$

$$\text{where } \bar\theta_{solid}=\int_{-1}^{0}\theta_{solid}dz\approx\theta_{solid} \text{ and } \sigma_{conj,mo}=\frac{kRa^{1/4}_{UWT,q'''}}{k_{solid}}$$

First, the case in which the longitudinal conduction dominated convection with $d/(L\sigma_{conj,mo})$ significantly greater than unity was considered. To solve the non-dimensionalized governing equation, the perturbation method was employed, in which θ_{solid} and θ are expanded as a power series in the parameter $d/(L\sigma_{conj,mo}) = \varepsilon$.

$$\theta_{solid}\approx\theta_{solid0}+\frac{1}{\varepsilon}\theta_{solid1}+\cdots \quad (14)$$

$$\theta\approx\theta_0+\frac{1}{\varepsilon}\theta_1+\cdots \quad (15)$$

Collecting terms of the same order, the following equations can be obtained.

$$\frac{\partial^2\theta_{solid0}}{\partial\chi^2}=0 \quad (16)$$

$$\frac{\partial^2\theta_{solid1}}{\partial\chi^2}=-1-\frac{1}{\chi^{1/4}}\left.\frac{\partial\theta_0}{\partial\eta}\right|_{\eta=0} \quad (17)$$

$$\frac{\partial^2\theta_{solidj}}{\partial\chi^2}=-\frac{1}{\chi^{1/4}}\left.\frac{\partial\theta_{j-1}}{\partial\eta}\right|_{\eta=0} \text{ for all } j>1 \quad (18)$$

$$\frac{\partial\theta_{solidj}}{\partial\chi}=0 \text{ at } \chi=0,1 \text{ for all } j \quad (19)$$

By integrating Eq. (17) along the χ direction, and applying Eq. (19), $d\theta_0/d\eta_0$ becomes -3/4. The leading-order variable of the fluid (θ_0) can be solved in terms of the solid temperature (θ_{solid}) using the existing similarity analyses.

$$\left.\frac{d\theta_0}{d\eta}\right|_{\eta=0}=-\frac{3}{4}\left[\frac{2\Pr}{5(1+2\Pr^{1/2}+2\Pr)}\right]^{1/4}\theta_{solid0}{}^{5/4}=-\frac{3}{4} \quad (20)$$

Considering the non-dimensionalization of Eq. (20), the heat flux is proportional to $x^{-1/4}$, similar to the case of the UWT solution, as shown in Eq. (21). Notably, when the longitudinal conduction dominated convection, the solution approached that of the UWT solution.

$$q''=-k\frac{\partial T}{\partial y}=\frac{3}{4}k\frac{\Delta T_{UWT,q'''}}{L}Ra^{1/4}_{UWT,q'''}\left(\frac{x}{L}\right)^{-1/4} \quad (21)$$

$$q''\sim x^{-1/4} \text{ for } \frac{d}{L\sigma_{conj,mo}}\sim\frac{\text{longitudinal conduction}}{\text{free convection}}>>1$$

Next, a case in which convection significantly dominated the longitudinal conduction, with $d/(Ls_{conj,mo})$ much less than unity, was considered. In this case, the first term on the left side of Eqs. (13) can be neglected, resulting in Eq. (22). Considering the non-dimensionalization of Eq. (22), the heat flux becomes constant, similar to that of the UHF solutions.

$$\left.\frac{d\theta_0}{d\eta}\right|_{\eta=0}=-\chi^{1/4} \quad (22)$$

$$q''=-k\frac{\partial T}{\partial y}=k\frac{\Delta T_{UWT,q'''}}{L}Ra^{1/4}_{UWT,q'''} \quad (23)$$

$$q''=\text{constant for } \frac{d}{L\sigma_{conj,mo}}\sim\frac{\text{longitudinal conduction}}{\text{free convection}}<<1$$

3. Numerical Evaluation

A numerical analysis of the nondimensional governing equations was conducted to examine the effect of the $d/(Ls_{conj,mo})$ value near unity. Eqs. (5) and (6), which represent free convective flows, can be expressed as a system of ordinary differential equations as shown in Eqs. (24) and (25), respectively. Here, the influence of longitudinal heat conduction on the flow is neglected.

$$F = \left[f_1, f_2, f_3, f_4, f_5 \right]^T = \left[f, f', f'', \theta, \theta' \right]^T \quad (24)$$

$$\frac{dF}{d\eta} = \left[f_2, f_3, -f_4 + \frac{1}{\Pr}\left(\frac{1}{2} f_2^2 - \frac{3}{4} f_1 f_3 \right), f_5, -\frac{3}{4} f_1 f_5 \right]^T \quad (25)$$

$$f_1(\eta = 0) = 0,\ f_2(\eta = 0) = 0 \quad (26)$$

$$f_2(\eta \to \infty) = 0,\ f_4(\eta \to \infty) = 0,\ f_5(\eta \to \infty) = 0 \quad (27)$$

For the above equations based on the Runge–Kutta method, initial conditions for f_3, f_4, and f_5 are necessary. Assuming that $f_4(0)$ is the wall temperature, Eq. (25) was calculated to satisfy boundary conditions in Eq. (27), and the wall velocity gradient $f_3(0)$ and wall heat flux $f_5(0)$ were determined. The MATLAB function ode15s was used to solve the differential equations.

Subsequently, the solid conduction was solved by integrating Eq. (13) along the χ direction. The discretization is illustrated in Fig. 2.

$$\int_w^e \left(\frac{d}{\sigma_{conj,mo} L} \frac{\partial^2 \theta_{solid}}{\partial \chi^2} + 1 \right) d\chi = \int_w^e \left(-\frac{1}{\chi^{1/4}} \left. \frac{\partial \theta}{\partial \eta} \right|_{\eta=0} \right) d\chi \quad (28)$$

$$\frac{d}{\sigma_{conj,mo} L} \left(\left. \frac{\partial \theta_{solid}}{\partial \chi} \right|_e - \left. \frac{\partial \theta_{solid}}{\partial \chi} \right|_w \right) + \Delta\chi + \frac{4}{3}\left(\chi_e^{3/4} - \chi_w^{3/4} \right) \left. \frac{\partial \theta}{\partial \eta} \right|_{\eta=0} = 0 \quad (29)$$

$$\frac{d}{\sigma_{conj,mo} L} \left(\frac{\theta_{solid,E} - \theta_{solid,P}}{(\delta\chi)_e} - \frac{\theta_{solid,P} - \theta_{solid,W}}{(\delta\chi)_w} \right) \quad (30)$$

$$+ \Delta\chi + \frac{4}{3}\left(\chi_e^{3/4} - \chi_w^{3/4} \right) \frac{\theta_{\eta=\Delta\eta} - \theta_{solid,P}}{\Delta\eta} = 0$$

$$a_p \theta_{solid,P} = a_E \theta_{solid,E} + a_W \theta_{solid,W} + b$$

$$\text{where } a_E = \frac{h}{\sigma_{conj,mo} L (\delta\chi)_e},\ a_W = \frac{h}{Bi_{mo} L (\delta\chi)_w}, \quad (31)$$

$$b = \Delta\chi + \frac{4}{3} \frac{\left(\chi_e^{3/4} - \chi_w^{3/4} \right) \theta_{\eta=\Delta\eta}}{\Delta\eta},$$

$$a_P = a_E + a_W + \frac{4\left(\chi_e^{3/4} - \chi_w^{3/4} \right)}{3\Delta\eta}$$

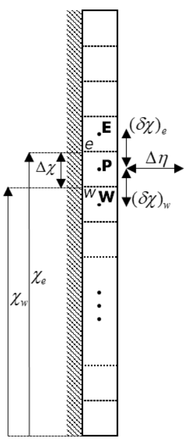

Fig. 2. Discretization of a free-convective vertical plate

In Eq. (30), $\Delta\eta$ and $\theta_{\eta=\Delta\eta}$ are obtained from the solutions of Eq. (24)–(27). The solid temperature (θ_{solid}) obtained from Eq. (30) is used as the input to solve Eq. (24)–(27), resulting in updated values for $\Delta\eta$ and $\theta_{\eta=\Delta\eta}$. This iterative calculation was repeated until the interface condition between the fluid and solid was satisfied. The iterative calculations for the fluid and solid regions are shown in Fig. 3.

Figs. 4(a) and (b) show the temperature profiles calculated numerically for Prandtl numbers of 1.0, and 10, respectively. As proposed in Section 2, the temperature profiles converged to the UWT solution when $d/(L\sigma_{conj,mo})$ was extremely large. When $d/(L\sigma_{conj,mo})$ was extremely small, the wall temperature was proportional to $\chi^{1/5}$, which is identical to that of the UHF solution. In addition, when the temperature profile converges to the UWT solution, the temperature values closely match the θ_{solid0} value in Eq. (20), as listed in Table 1.

The heat flux profiles are presented in Figs. 5(a) and (b) for Prandtl numbers 1.0 and 10, respectively. Similarly, the heat-flux profiles converged to the UHF solution when $d/(L\sigma_{conj,mo})$ was small. In cases where $d/(L\sigma_{conj,mo})$ is large, the heat flux is proportional to $\chi^{-1/4}$, which is identical to the UWT solution in Eq. (3). Interestingly, the non-dimensional temperature is affected by the Prandtl number, whereas the non-dimensional heat flux is not influenced by the Prandtl number, as derived in the analytic solutions of Eqs. (20), (21), and (23).

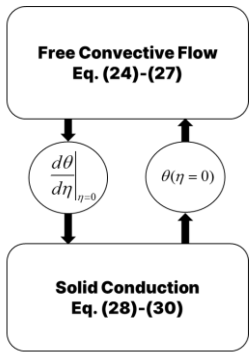

Fig. 3. Iterative calculation matching interface conditions

(a)

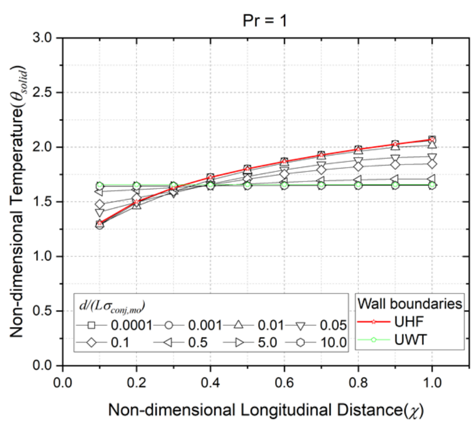

(b)

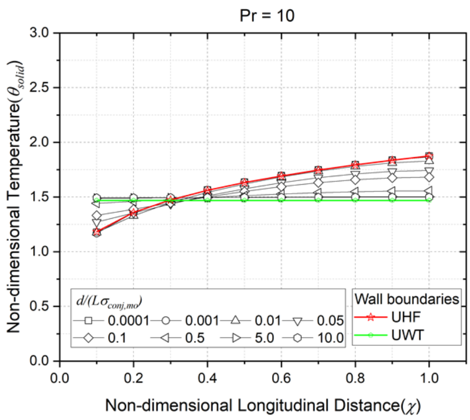

Fig. 4. Profiles of non-dimensional temperature for (a) Pr = 1.0 and (b) Pr = 10

(a)

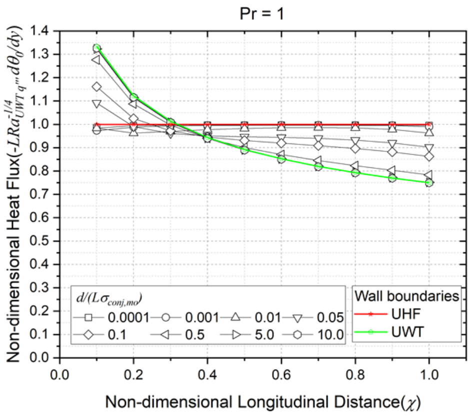

(b)

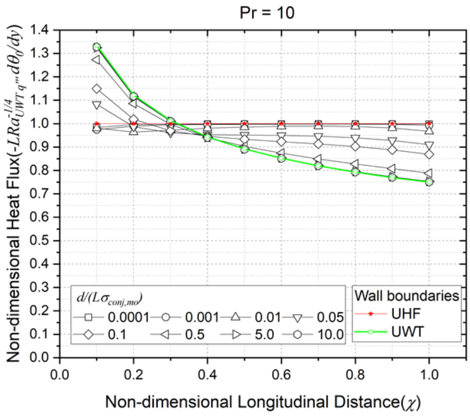

Fig. 5. Profiles of non-dimensional heat flux for (a) Pr = 1.0 and (b) Pr = 10

Table 1. Comparison of θ_{solid0} for UWT calculated analytically and numerically

	Pr=0.1	Pr=1.0	Pr=10
Numerical θ_{solid0} for UWT	2.073	1.651	1.499
Analytical θ_{solid0} for UWT in Eq. (20)	2.149	1.657	1.469

In conclusion, when the longitudinal conduction is much more dominant than the free convection represented by the nondimensional parameter *d/(Lσ*$_{conj,mo}$*)*, the solutions converge to the UWT solution. Conversely, when the convection was significantly more dominant than the longitudinal conduction, the solution converged to the UHF solution. The specific criteria are expressed in Eq. (32).

$$\frac{1}{\sigma_{conj,mo}}\frac{d}{L} \sim \frac{\text{longitudinal conduction}}{\text{free convection}} < 0.01 \ \text{: Converge to UHF solution} \quad (40)$$

$$\frac{1}{\sigma_{conj,mo}}\frac{d}{L} \sim \frac{\text{longitudinal conduction}}{\text{free convection}} > 0.5 \ \text{: Converge to UWT solution}$$

4. Conclusions

This study proposed evaluations for the wall boundary conditions of free convective thin plates with volumetric heat generation using analytical and numerical approaches. The key findings indicate that the non-dimensional parameter $d/(L\sigma_{conj,mo})$ determines the dominant thermal boundary behavior, with values above 0.5 leading to uniform wall temperature (UWT) conditions and those below 0.01 resulting in uniform heat flux (UHF) conditions. Numerical analyses confirmed that while the Prandtl number affects the temperature distribution, it has minimal impact on heat flux profiles. Additionally, the study found that UHF conditions result in the highest peak temperatures, while UWT conditions yield the lowest. These insights provide practical guidelines for optimizing material selection and plate dimensions to achieve desired thermal boundary conditions in thermal design of fuel assemblies.

REFERENCES

[1] A.W.M.R. Bar-Cohen, "Thermally Optimum Spacing of Vertical, Natural Convection Cooled, Parallel Plates," ASME Journal of Heat Transfer, **106**(1), pp. 116-123, 1984.
[2] A. Bejan, et al., "The Cooling of a Heat-Generating Board Inside a Parallel-Plate Channel," *International Journal of Heat and Fluid Flow*, **14**(2), pp. 170-176, 1993.
[3] W. Kays, M. Crawford, and B. Weigand, "Chapter 17. Convective Heat Transfer With Body Forces," in *Convective Heat and Mass Transfer*, pp. 367-398, 2005.